Applied Catalysis B: Environmental 127 (2012) 182–189

Contents lists available at SciVerse ScienceDirect

Applied Catalysis B: Environmental

journal homepage: www.elsevier.com/locate/apcatb

Heterogeneous oxidation of naproxen in the presence of α-MnO_2 nanostructures with different morphologies

Yiping Zhang, Yulong Yang, Yan Zhang, Tuqiao Zhang, Miaomiao Ye*

Institute of Municipal Engineering, Zhejiang University, Hangzhou 310058, PR China

ARTICLE INFO

Article history:
Received 8 February 2012
Received in revised form 20 June 2012
Accepted 16 August 2012
Available online 30 August 2012

Keywords:
Manganese oxide
Pharmaceutical and personal care products
Naproxen
Heterogeneous oxidation
Nanostructures

ABSTRACT

α-MnO_2 nanostructures with different morphologies including nanoparticles, flower-like nanostructures and nanorods have been successfully prepared and used in the heterogeneous oxidation of naproxen in water. It has been found out that the heterogeneous oxidation process is highly pH dependent, with higher efficiency at lower pH values. The oxidation kinetics of naproxen were modeled by Langmuir–Hinshelwood equations. Based on the kinetic constants (k), the oxidation efficiency follows the order of commercial particles < nanorods < flower-like nanostructures < nanoparticles. The mechanism for the oxidation of naproxen has been studied in depth, which shows that the high efficiency can be ascribed to the specific adsorption, electron transfer, and byproducts release. Dissolved anions (Cl^-, CO_3^{2-}, SO_4^{2-}, PO_4^{3-}) and cations (Mn^{2+}) could remarkably decrease the removal rate by competitively adsorbing and reacting with MnO_2, respectively. In addition, a total of 7 byproducts were identified by LC–MS from which a tentative pathway was proposed.

1. Introduction

The widespread use of pharmaceutical and personal care products (PPCPs) in daily life unavoidably results in their release into the aquatic environment [1,2]. Consequently, more than 80 PPCPs have been detected in wastewater, surface water, groundwater, and drinking water throughout the world [3–5]. Although the adverse impact of PPCPs on human health or environment is still not fully understood, PPCPs are regarded as being potentially hazardous compounds even at trace concentrations since some of PPCPs may cause disruption of endocrine systems and affect the hormonal control of development in aquatic organisms, wildlife and humans [6–8]. PPCPs in wastewater therefore must be removed or decomposed before the discharge of wastewater. Unfortunately, it is reported that conventional water treatment processes such as coagulation, sedimentation, filtration, chlorination and biodegradation cannot satisfy with the PPCPs removal [9–11]. It is therefore essential to develop new approaches to remove PPCPs with high efficiency.

Up to now, new physicochemical approaches including adsorption, membrane separation, photodegradation, photocatalysis, ozonation, etc. [12–16], have been adopted to remove PPCPs from drinking water or wastewater. Besides these processes, heterogeneous oxidation using manganese oxide is another efficient method for the elimination of organic pollutants [17–22]. Manganese oxides exhibit considerable activity in oxidation–reduction reactions due to the presence of manganese ions with different oxidation states [23]. It has been reported that manganese oxides can oxidize a number of model organic compounds [24,25]. For example, Stone [17] reported the oxidation of substituted phenols by manganese (III/IV) oxides and proposed a possible oxidation mechanism. Huang and co-workers [26] observed that manganese dioxide formed in situ had a significantly high adsorption capacity for several hazardous aromatics. Gan and co-workers [27] described that natural occurring MnO_2 had the capability to oxidize bisphenol F (BPF), in which the oxidation process was found to be dependent closely on pH and to be inhibited by cosolutes including organic matter, cations and anions. Zhao and co-workers [28] proved that chlortetracycline (CTC) can be efficiently degraded by δ-MnO_2, and the byproducts formed in the reaction system were less toxic than that of CTC. However, to the best of our knowledge, no report on the removal of PPCPs by heterogeneous oxidation processes using α-MnO_2 with different morphologies as the oxidants have been published. In this paper, the heterogeneous oxidations of naproxen in the presence of α-MnO_2 nanostructures with different morphologies including nanoparticles, flower-like nanostructures and nanorods were studied. Naproxen is a non-steroidal anti-inflammatory drug (NSAID) that is widely used for reduction of pain, fever, inflammation and stiffness. It was selected as a representative of PPCPs since it has been widely detected in the aquatic environment [29,30]. The reaction kinetics and reaction pathways were explored. Parameters affecting the oxidation process such as initial solution pH and inorganic ions were investigated. Moreover,

* Corresponding author. Tel.: +86 571 88208721; fax: +86 571 88208721.
E-mail address: yemiao008@zju.edu.cn (M. Ye).

0926-3373/$ – see front matter © 2012 Elsevier B.V. All rights reserved.
http://dx.doi.org/10.1016/j.apcatb.2012.08.014

the mechanism for the removal of naproxen was also discussed. Finally, the stability of the α-MnO_2 nanorods was monitored by following the evolution of their oxidation activity during six cycles of use.

2. Experimental

2.1. Chemicals

All reagents were used in the same condition as they were received from the manufacturers. Naproxen (99%) was purchased from Alfa Aesar. Potassium permanganate ($KMnO_4$, >99%) and manganese sulfate ($MnSO_4$, >99%) were purchased from Meixing Chemical Co., Ltd. (Shanghai, China). High performance liquid chromatographic (HPLC)-grade methanol and acetonitrile were purchased from Sigma–Aldrich. Other reagents such as sodium chloride (NaCl), calcium chloride ($CaCl_2$), manganese chloride ($MnCl_2$), aluminum chloride ($AlCl_3$), sodium carbonate (Na_2CO_3), sodium sulfate (Na_2SO_4) and sodium phosphate (Na_3PO_4) with reported purities >98% were purchased from Sinopharm Chemical Reagent Co., Ltd. (Shanghai, China). Ultrapure water was obtained from Ultrapure Water System (arium 611UF, Sartorius Stedim Biotech GmbH). Naproxen stock solution was prepared in deionized water at 5.0×10^{-5} mol/L and stored in a 1 L brown volumetric flask at 4 °C.

2.2. Synthesis of α-MnO_2 nanostructures with different morphologies

The synthesis of α-MnO_2 nanostructures with different morphologies was carried out using a modified hydrothermal procedure [31]. Typically, 20 mL of $KMnO_4$ (0.2 mol/L) was mixed with 16 mL of $MnSO_4$ (0.125 mol/L) and stirred for 5 min. The final mixture was then directly transferred into a 50 mL Teflon-lined stainless autoclave, which was maintained at 160 °C for 0, 1, and 24 h, respectively, and then allowed to cool to room temperature naturally. The brown precipitate was collected, washed with distilled water and ethanol three times, respectively, and then air-dried at 80 °C for 12 h.

2.3. Characterization of α-MnO_2 nanostructures

The crystalline structures of the products were evaluated by X-ray diffraction (XRD) analyses, carried out on a Rigaku D/max-rA diffractometer with Cu Ka radiation (λ = 1.5405 Å). The morphologies of the products were analyzed using a Hitachi S-4800 scanning electron microscope (SEM) and a Phillips Tecnai 10 transmission electron microscope (TEM) with an accelerating voltage of 100 kV. The BET surface area and pore size distribution of the products were measured by N_2 adsorption–desorption test (Quantachrome, ASIC-2 measuring instrument). Point of zero charge (pzc) of the α-MnO_2 nanorods was determined using a Malvern zeta sizer nano-Z instrument.

2.4. Batch oxidation experiments

Heterogeneous oxidations of naproxen were carried out in batch mode in a thermostated room at 25 °C. A 60 mL reaction slurry, prepared with a given amount of α-MnO_2 0.5 g/L and naproxen in concentration of 1.0×10^{-5} mol/L, was added to a 100 mL conical flask. The initial solution pH range from 2.50 to 10.00 was adjusted with sodium hydroxide and/or hydrochloric acid. Agitation was provided by magnetic stirrer at a stirring rate of 400 rpm. 6 mL of suspension was collected at timed intervals with a 10 mL syringe. Then the sample was immediately filtrated through a 0.45 μm filter for analysis of naproxen concentration and dissolved manganese. The effects of the naproxen concentration on the naproxen removal were carried out by varying the initial concentrations of naproxen from 1.0×10^{-5} to 5.0×10^{-5} mol/L with the MnO_2 dosage of 0.5 g/L while keeping other reaction conditions unchanged. For recycling use of the oxidant, after the α-MnO_2 nanorods were separated from solution by filtration, the clear upper solution was removed and the nanorods was redispersed in naproxen solution (60 mL) by sonication. The effects of inorganic ions were carried out in the presence of α-MnO_2 nanorods at [ions] = 5.0×10^{-4} mol/L, $[naproxen]_0 = 1.0 \times 10^{-5}$ mol/L, $[\alpha\text{-}MnO_2]_0 = 0.5$ g/L, and pH 2.5 with different inorganic ions (Na^+, Ca^{2+}, Mn^{2+}, Al^{3+}, Cl^-, CO_3^{2-}, SO_4^{2-} and PO_4^{3-}).

2.5. Analysis of naproxen, TOC, Mn^{2+}, and byproducts

The concentration of naproxen was determined by HPLC (Agilent 1200, USA) provided with a UV–vis detector. A 4.6 mm × 250 mm (5 μm) XDB-C_{18} column was used. The analysis was carried out with a 70/30 (v/v) acetonitrile/water mobile phase and the flow rate was set at 1.0 mL/min. The injection volume was 10 μL. The progress of the mineralization of naproxen was monitored by measuring the total organic carbon (TOC) concentration via a TOC analyzer (TOC-V_{CPH}, Shimadzu, Japan). The concentration of the Mn^{2+} dissolved in the solution was determined by using a Thermo ICE3500 Atomic Absorption Spectrometer. In order to obtain sufficient amounts of all possible intermediates for analysis, the oxidation process was investigated at initial concentrations of naproxen of 5.0×10^{-5} mol/L and α-MnO_2 dosage of 0.5 g/L. The reaction intermediates and byproducts were analyzed by using an Agilent 6460 triple quadrupole high performance liquid chromatography mass spectrometry. The mass spectrometric measurements were carried out using an electrospray ionization source in positive ion mode. A Zorbax SB C_{18} column (2.1 mm × 150 mm, 5 μm) was used to separate naproxen and the intermediates. The analysis was carried out with a 38/62 (v/v) acetonitrile/water mobile phase and the flow rate was set at 0.3 mL/min. MS source setting: gas temperature: 325 °C; gas flow: 5 L/min; nebulizer: 45 psi; sheath gas temperature: 250 °C; sheath gas flow: 11 L/min; capillary voltage: 4000 V(+); nozzle voltage: 500(+); fragmentor: 135 V.

3. Results and discussion

3.1. Characterization of α-MnO_2 with different morphologies

The XRD patterns of as-prepared samples obtained at different hydrothermal treatment times are shown in Fig. 1. The material prepared at room temperature shows an amorphous MnO_2 having peaks evolving to an α-MnO_2 structure [32]. After hydrothermal treatment at 160 °C for 1 h, the broad peak features show the mixture of amorphous and nanocrystalline nature of the sample. With the hydrothermal treatment time further increased to 24 h, the strong and sharp diffraction peaks indicate that the sample is highly crystalline (as shown in Fig. 1c). All diffraction peaks can be readily indexed to a pure tetragonal phase of α-MnO_2 with lattice constants a = 9.7847 Å and c = 2.8630 Å (JCPDS 44-0141). No characteristic peaks of other impurities are detected in the XRD patterns, suggesting that the successful preparation of α-MnO_2 with high purity.

The morphologies and microstructures of the α-MnO_2 prepared at various hydrothermal treatment times were characterized by scanning electron microscopy (SEM) and transmission electron microscope (TEM). It can be clearly noticed that direct mixing of $KMnO_4$ and $MnSO_4$ leads to the formation of a precipitate of MnO_2 (see Fig. 2a). The flower-like nanostructures can be observed after

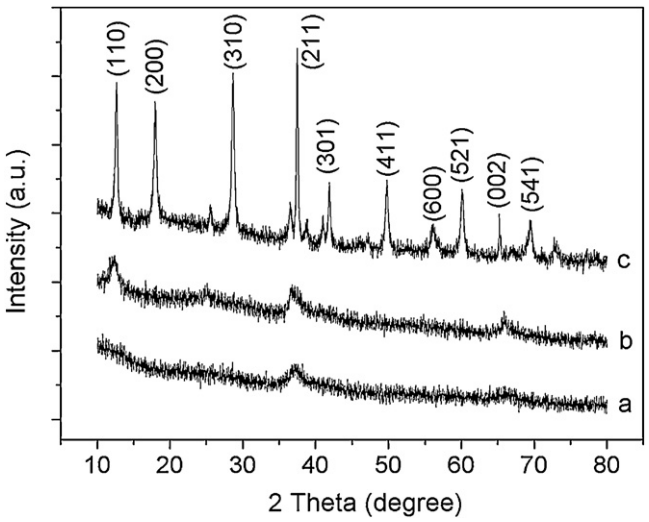

Fig. 1. XRD patterns of α-MnO_2 after hydrothermal treatment at 160 °C for (a) 0 h, (b) 1 h, and (c) 24 h, respectively.

1 h of hydrothermal treatment at 160 °C. As shown in Fig. 2b and c, the subsequent increase in the hydrothermal treatment time not only increases the crystallinity of the α-MnO_2 but also leads to the morphology transformation from flower-like structures to rod-like structures. The corresponding TEM images of the α-MnO_2 nanostructures with different morphologies are shown in Fig. 2d–f. The average sizes of the nanoparticles and flower-like nanostructures are ~30 nm and ~400 nm, respectively. Moreover, the average diameter of the nanorods is about 55 nm with the length ranging from 0.65 to 7.5 μm, which is in good agreement with the SEM observation.

The surface areas and the pore structures of the as-prepared samples were investigated by measuring the nitrogen adsorption–desorption isotherms. Fig. 3a shows the nitrogen adsorption–desorption isotherms of the α-MnO_2 nanostructures with different morphologies. Without hydrothermal treatment, the isotherms are of the typical type IV pattern with distinct H_2 and H_3 hysteretic loops in the range of 0.4–0.8P/P_0 and 0.9–1.0P/P_0, respectively, indicating the existence of ink-bottle- and slit-shaped pores according to the IUPAC classification [33]. It has proven that the bimodal pore structures are beneficial to the enhancement of oxidation efficiency due to faster diffusion of various reactants and byproducts [34–36]. With increasing hydrothermal treatment time, the two small hysteresis loops merge into a big one and the area of the hysteresis loop gradually became bigger, which indicates the disappearance of the bimodal pore structures and the increase of the total pore volume, respectively. However, the hysteresis loop nearly disappeared when further increases the hydrothermal treatment time to 24 h, suggesting the non-porous structures of the sample. This is because of the morphology transformation from flower-like nanostructures to nanorods (as shown in the SEM images). The corresponding pore size distributions of the α-MnO_2 nanostructures with different morphologies (see Fig. 3b) were determined using the Barrett–Joyner–Halenda (BJH) method from the desorption branch of the isotherm. Data concerning the BET surface areas, total pore volumes and average pore sizes of different samples are present in Table 1. Obviously, the increase in the hydrothermal treatment time leads to a reduction in the BET surface area while increasing the average pore size.

3.2. Heterogeneous oxidation of naproxen

3.2.1. Effect of morphology and pH on the degradation reaction

The naproxen removal rates at reaction time of 24 h in the presence of α-MnO_2 with different morphologies including

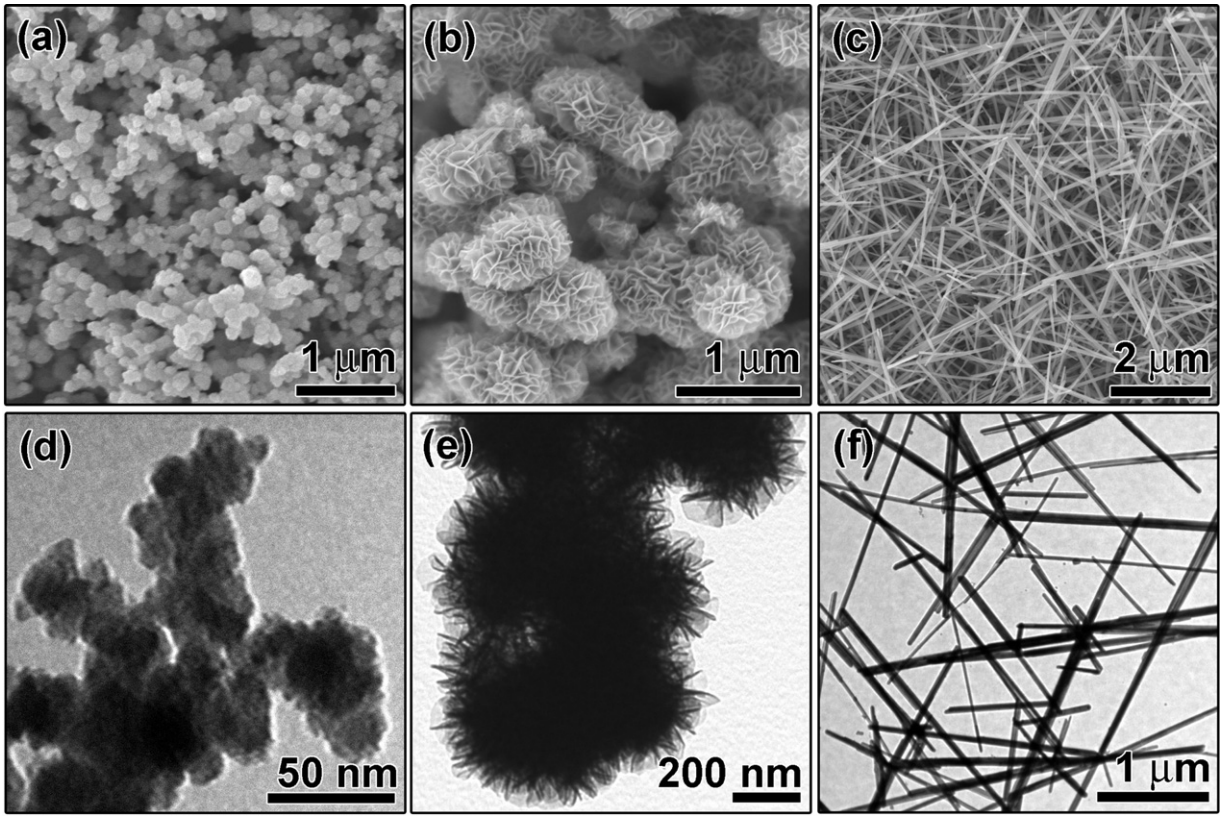

Fig. 2. SEM and TEM images of α-MnO_2 after hydrothermal treatment at 160 °C for (a, d) 0 h, (b, e) 1 h, and (c, f) 24 h, respectively.

Table 1
BET surface areas and pore structures of the α-MnO_2 nanostructures with different morphologies.

Samples	BET surface area (m^2/g)	Average pore size (nm)	Total pore volume (cm^3/g)
Nanoparticles	135.0	6.02	0.21
Flower-like	69.5	11.70	0.24
Nanorods	22.5	12.17	0.072

Table 2
Langmuir–Hinshelwood kinetic (k) and Langmuir adsorption (K) constants of the α-MnO_2 nanostructures with different morphologies and commercial particles.

Samples	k (mmol/(L h))	K (L/mmol)	R^2
Nanoparticles	1.09	4.43	0.997
Flower-like	0.23	9.13	0.981
Nanorods	0.11	11.63	0.999
Commercial	0.026	15.73	0.946

nanoparticles, flower-like nanostructures and nanorods at different pH levels are shown in Fig. 4, from which one can see obviously that the oxidation processes of the naproxen over α-MnO_2 nanostructures are highly pH dependent. The oxidation efficiency decreases with increase of the pH values. Taking the nanorods as an example, complete removal of naproxen can be observed at pH ≤ 2.5, while none of the naproxen is removed at pH ≥ 7.8. A mechanism for the reaction of organic compounds with manganese (III/IV) oxide surfaces has been presented by Stone [17,23], which can be described involving the specific adsorption of organic compound onto the particle surface to first form a surface precursor complex, followed by electron transfer and byproducts release. The α-MnO_2 nanorods have a zero potential point of pH 3.15 (which is very close to that of the reported one [18]; inset of Fig. 4). Therefore, the surface of α-MnO_2 nanorods is negatively charged at pH values above 3.15, while positively charged when pH values is below 3.15. In addition, it has been pointed out that carboxylic acids are adsorbed more effectively at low pH values, generally lower than the pKa of the corresponding acids, where they are present at their undissociated forms [37,38]. For naproxen, with the pKa of ~4.2 [39], the undissociated form can be adsorbed on the surface of α-MnO_2 nanorods more easily in comparison with its corresponding dissociated form. Therefore, the removal efficiency remarkably increases as the pH decreases from 4.86 to 2.5. At pH ≥ 7.8, the removal efficiency of the naproxen is negligible, which can be well explained by the electrostatic repulsion between the dissociated form of naproxen and the deprotonation of α-MnO_2. Moreover, coupled with the oxidation of naproxen, Mn^{2+} was generated by reduction of α-MnO_2 nanorods. The generated Mn^{2+} could be adsorbed on the negatively charged MnO_2 surface, which in turn slows down the reaction rate [28,40].

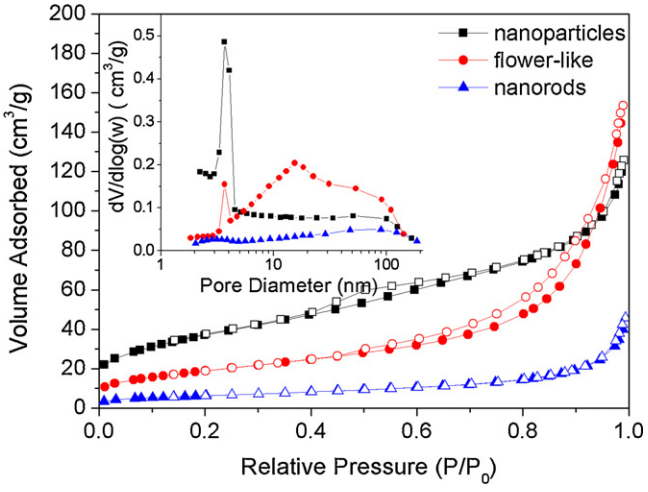

Fig. 3. Nitrogen adsorption–desorption isotherms of the α-MnO_2 with different morphologies. The inset shows their BJH pore size distribution curves.

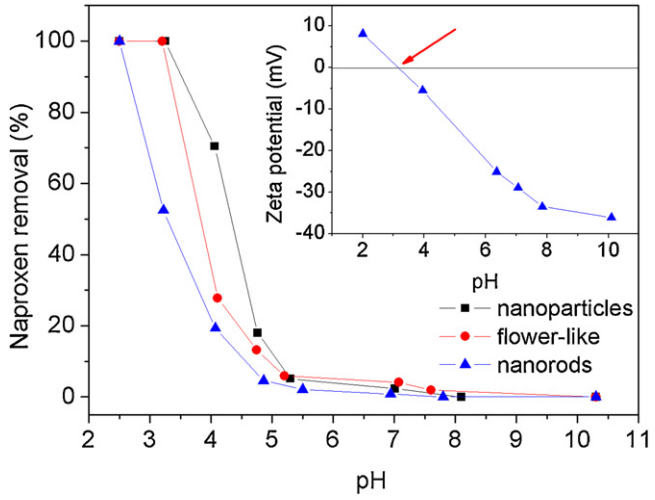

Fig. 4. (a) Effect of pH on the naproxen removal rates in the presence of three different oxidants at $[naproxen]_0 = 1.0 \times 10^{-5}$ mol/L, $[\alpha\text{-}MnO_2]_0 = 0.5$ g/L. The inset shows the zeta potential of α-MnO_2 nanorods as a function of pH in 1.0×10^{-3} mol/L NaCl solution.

The oxidation kinetics of naproxen by α-MnO_2 nanostructures with different morphologies and commercial MnO_2 particles are generally modeled by the Langmuir–Hinshelwood (L–H) models, which can be represented as follows:

$$r_0 = \frac{kKC_0}{1 + KC_0} \quad (1)$$

where r_0 is the initial reaction rate (mmol/(L h)), k the reaction kinetic constant (mmol/(L h)), and K is the Langmuir adsorption constant (L/mmol). The initial reaction rates (r_0) were calculated for each experiment by modeling the kinetics of oxidation by a nonlinear fitting equation (as shown in Fig. S1, Supporting information) and its derivative form at initial time $r_0 = (dC/dt)_{t=0}$. Fig. 5 shows the experimental points modeled by the L–H equation for the α-MnO_2 nanostructures with different morphologies and commercial MnO_2 particles. The kinetic constants (k) and the Langmuir adsorption constant (K) for the α-MnO_2 nanostructures with different

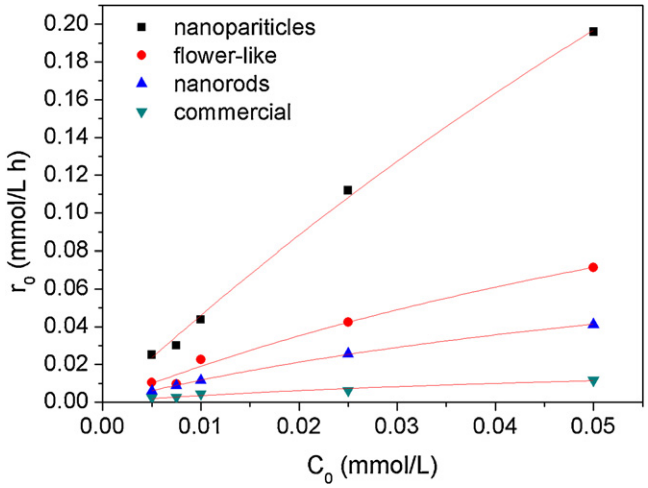

Fig. 5. Evolution of the initial reaction rate (r_0) as a function of initial concentration (C_0) and the reference modeled by Langmuir–Hinshelwood equation.

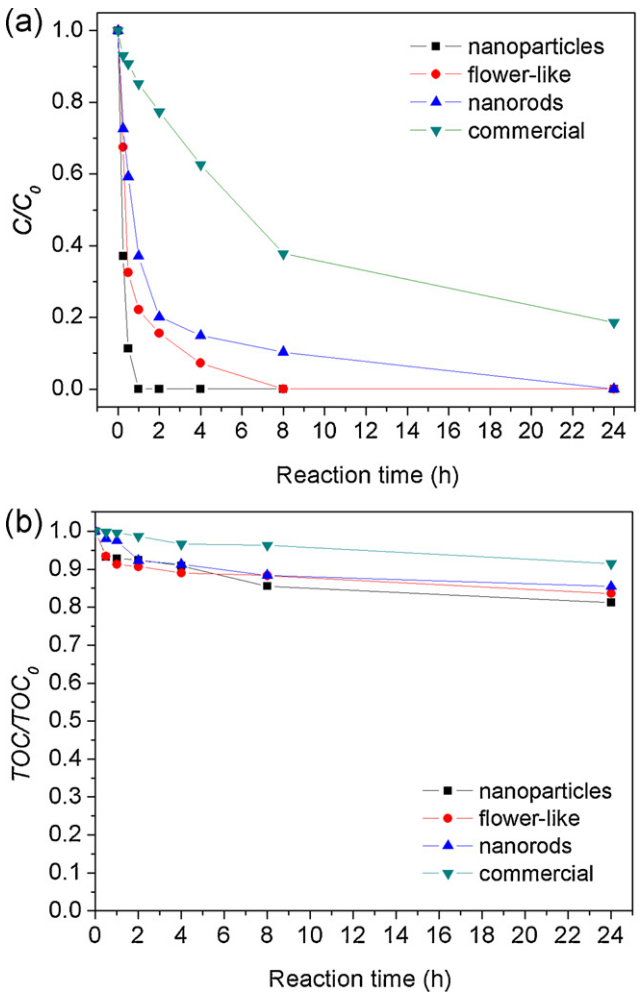

Fig. 6. (a) Naproxen removal and (b) TOC removal at solution pH value of 2.5 in the presence of α-MnO_2 with different morphologies and commercial MnO_2 particles, respectively.

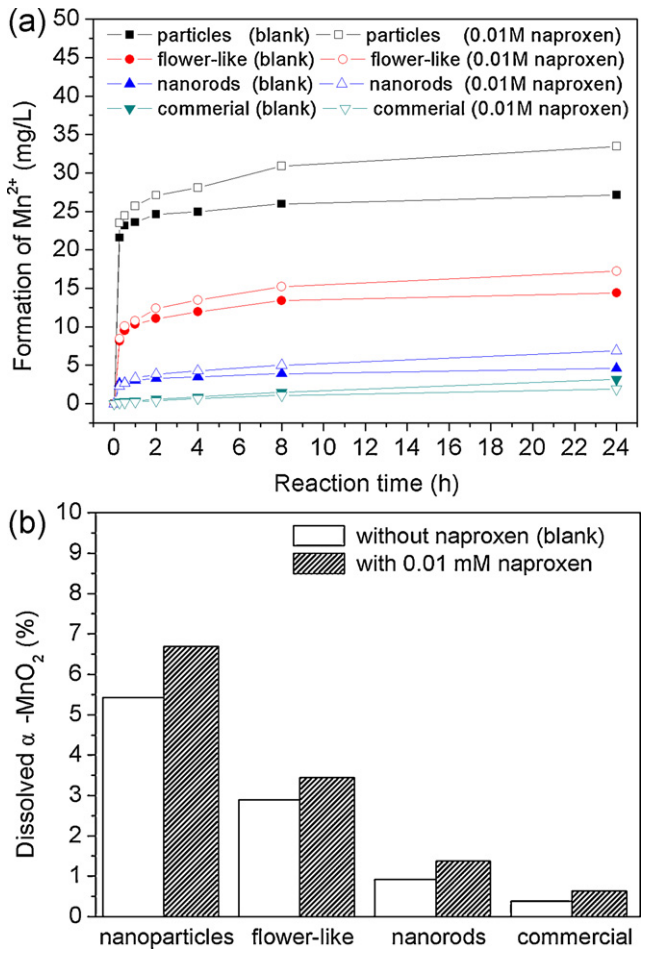

Fig. 7. (a) Formation of Mn^{2+} and (b) dissolved α-MnO_2 in these two oxidation processes with and without naproxen by using MnO_2 particles, flower-like structures, and nanorods as the oxidants, respectively.

morphologies and commercial particles are summarized in Table 2. Based on the kinetic constants (k), the oxidation efficiency follows the order of commercial particles < nanorods < flower-like nanostructures < nanoparticles. On the other hand, the Langmuir adsorption constant (K) follows the order of nanoparticles < flower-like nanostructures < nanorods < commercial particles. Herein, the reason that α-MnO_2 nanoparticles possesses the best oxidation efficiency is not only due to its larger surface area and highly amorphous nature for the fast and vast adsorption of the naproxen [40] but also due to its bimodal pore structures for the faster release of byproducts [34]. In addition, the total organic carbon (TOC) was monitored to obtain some useful information about the oxidation efficiency of the reactions and the mineralization of the naproxen. The results are shown in Fig. 6, from which one can see that the TOC removal rate is correspondingly lower than its concentration removal rate. No more than 20% mineralization of the naproxen are reached at the reaction time of 24 h in all of these four oxidation processes, indicating the existence of other organic byproducts in the reaction systems. The possible intermediates and byproducts were analyzed by LC–MS, and the detailed results will be discussed later. In general, it has been proved that MnO_2 heterogeneous oxidation mainly contributes to the concentration removal and the increase of biodegradability, although it also leads to the small portion of TOC removal [18,41,42].

The correspondingly dissolved manganese in the reaction solution was monitored to demonstrate one of the products released during the reaction, and also to confirm the oxidation mechanism. The appearance of Mn^{2+} can be observed from the early stage of these two oxidation processes with and without naproxen (as shown in Fig. 7a). The concentration of Mn^{2+} in the oxidation process with naproxen is always higher than that in the blank experiment, and the quantitative difference of the Mn^{2+} concentration gradually increases as the reaction processes. This phenomenon indicates that the MnO_2 can not only provide reactive sites for adsorption, but also trap electrons for oxidation, thus further proving the oxidation mechanism mentioned above. Additionally, the quantitative difference of the Mn^{2+} concentration in these four different oxidation processes follows the order of commercial particles < nanorods < flower-like nanostructures < nanoparticles means that the oxidation efficiency follows the order of commercial particles < nanorods < flower-like nanostructures < nanoparticles. However, in the blank experiments, the concentration of Mn^{2+} in the solution was measured at 27.15 and 14.43 mg/L when using α-MnO_2 nanoparticles and flower-like nanostructures as the oxidants, respectively, which was about 5.43% and 2.89% of total catalysts dosage in the system (out of a total of 500 mg in 50 mL solution; Fig. 7b). Too much MnO_2 were dissolved in the solution indicates that the instability of these two kinds of oxidants. The dissolved manganese not only causes the loss of the oxidant but also causes the secondary pollution of the water. Therefore, the α-MnO_2 nanorods were selected as the oxidant in the subsequent study due to its better chemical stability and higher

oxidation efficiency when compared with α-MnO_2 nanoparticles and commercial MnO_2, respectively.

3.2.2. Effect of inorganic ions

It has been reported that some of the anions and cations can be adsorbed on the surface of the manganese oxides to occupy the active surface sites, thereby slowing reaction rates [28,40]. In order to quantify such an effect on naproxen removal, a series of experiments were carried out by adding different anions and cations to the reaction systems. It can be seen from Fig. S2, Supporting information, that the addition of anions (Cl^-, CO_3^{2-}, SO_4^{2-}, PO_4^{3-}) considerably decreased the reaction rate of naproxen oxidation by α-MnO_2 nanorods. The obviously inhibitory effects of anions are caused by their competitions with naproxen for occupation of the active surface sites of α-MnO_2 nanorods. No significant inhibition effect was observed with the addition of these three cations (Na^+, Ca^{2+}, and Al^{3+}, as shown in Fig. S3, Supporting information). Because these three cations are less likely to adsorb on the α-MnO_2 nanorods surface due to repulsive forces. However, the presence of Mn^{2+} cations significantly decreases the reaction efficiency. The inhibition effect of Mn^{2+} is caused not only due to its reaction with Mn^{4+} for lowering the average oxidation state of MnO_2 [28,43,44], but also due to its "auto-inhibiting effect" for slowing the reaction rate [40].

3.2.3. Recycling

One-dimensional nanostructures have the advantage over powder catalysts in the easiness of separating the catalyst from solution by filtration or sedimentation [45]. In our experiment, the α-MnO_2 nanorods can be separated from an aqueous suspension in less than 30 min by sedimentation. The stability of the as-prepared

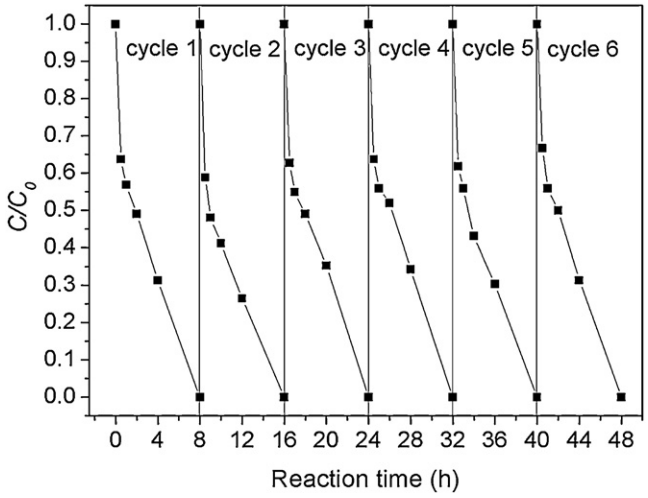

Fig. 8. Six cycles of the heterogeneous oxidation of naproxen in the presence of α-MnO_2 nanorods at $[naproxen]_0 = 1.0 \times 10^{-5}$ mol/L, $[\alpha\text{-}MnO_2]_0 = 0.5$ g/L, and pH = 2.5.

α-MnO_2 nanorods was tested by monitoring the oxidation activity during six cycles of use, as shown in Fig. 8, from which one can see that the oxidant do not exhibit any significant loss of oxidation activity even after six cycles of reaction. Though there is a weight loss of about 1.38% of total α-MnO_2 nanorods in the system, the morphologies of the α-MnO_2 nanorods after 1-time and 6-time cycling uses were unchanged (as shown in Fig. S4, Supporting information), which indicates that the chemical stability of the α-MnO_2 nanorods is good and also confirms that the oxidation reaction is happened in the surface of the nanorods.

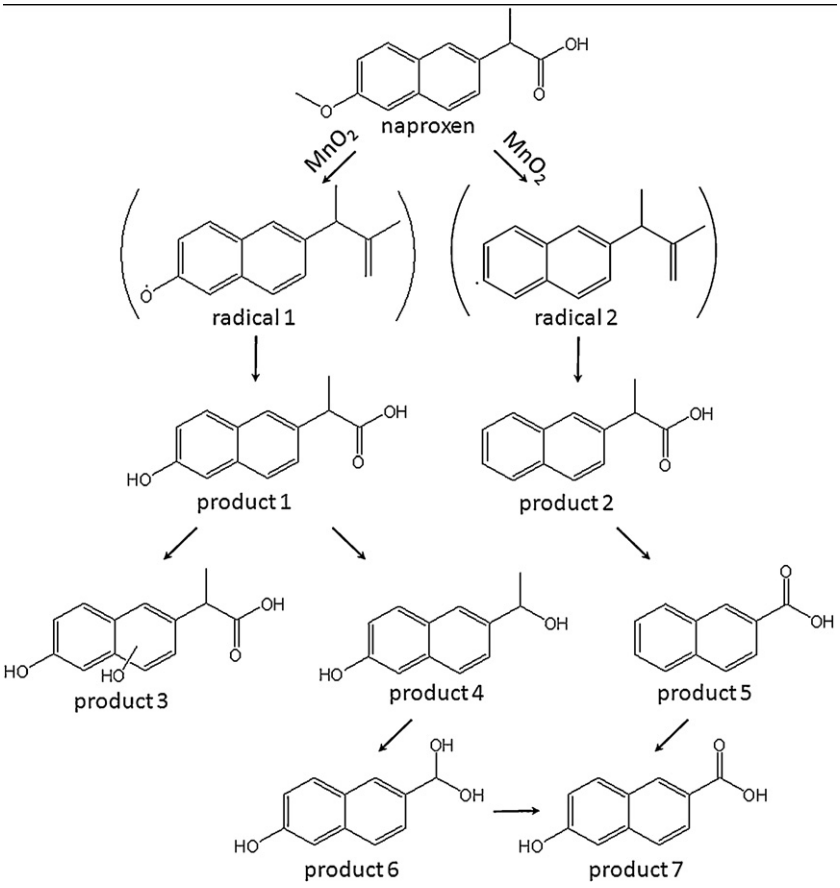

Fig. 9. A possible reaction pathway describing the oxidation of naproxen by α-MnO_2 nanorods.

3.3. Oxidation products and pathways

As mentioned above, the mineralization of naproxen is not complete in the reaction system, indicating the formation of other organic byproducts. To further identify these different organic byproducts, the liquid chromatography–mass spectrometric (LC–MS) measurements were carried out using an electrospray ionization source in positive ion mode. The HPLC chromatograms of the solution recorded at the reaction time of 0, 1, and 4 h are shown in Fig. S5 (Supporting information), from which one can clearly notice the presence of several byproducts. Most of them presented short retention time when compared to that of naproxen ($t_{retention}$ = 7.42 min). The parent compound naproxen and 7 byproducts were tentatively identified by mass spectrometry in positive mode (as shown in Fig. S6, Supporting information). The parent compound naproxen had the pseudo-molecular ion $[M+H]^+$ with m/z 230 yielding two major fragments m/z 185 and 158. The fragment m/z 185 and 158 was formed due to the loss of formyl group (CHO_2) and propionyloxy group ($C_3H_6O_2$), respectively. Based on the structures of these 7 byproducts, a tentative pathway was proposed (see Fig. 9). In the proposed pathway, naproxen transfers electrons to α-MnO_2 and forms two types of radicals (radical 1 and radical 2 in Fig. 9), and these two radicals then capture hydrogen atoms to form product 1 and product 2, which are further oxidized to form products 3, 4 and 5, respectively. Further oxidation results in the formation of products 6 and 7. The oxidation efficiency of manganese oxide is not good enough for complete mineralization of organic compounds as reported by other researchers [18,41,42]. The proposed reaction pathway describing the oxidation of naproxen (as shown in Fig. 9) is based on the LC–MS data of the solution recorded at the reaction time of 1, 4, and 8 h. We therefore believe that the naphthalene derivatives are the main byproducts since the ring open products can hardly be formed during the MnO_2-based oxidation process. The small portion (no more than 20%) of the TOC removal can be explained by the adsorption of the intermediates on the surface of the α-MnO_2.

4. Conclusions

In summary, α-MnO_2 nanostructures with different morphologies including nanoparticles, flower-like nanostructures and nanorods were employed to oxidation of naproxen in water. The α-MnO_2 nanorods not only exhibits higher oxidation efficiency than that of the commercial MnO_2 but also processes better chemical stability than that of the α-MnO_2 nanoparticles and flower-like nanostructures. The oxidation kinetics of naproxen by α-MnO_2 nanostructures can be fitted to the Langmuir–Hinshelwood model. The addition of anions (Cl^-, CO_3^{2-}, SO_4^{2-}, PO_4^{3-}) and cations (Mn^{2+}) can decrease the reaction efficiency of naproxen by competitive inhibition of adsorption on α-MnO_2 nanorods surfaces or reaction with α-MnO_2 nanorods, respectively. The incomplete mineralization of naproxen reveals that the formation of organic byproducts in the reaction system. In addition, it has been demonstrated that the α-MnO_2 nanorods can be recycled without decreasing its oxidation activity after 6-time cycling. Overall, the as-described α-MnO_2 nanorods are efficient and potential oxidants in the industrial application of the removal of naproxen in water.

Acknowledgments

This work was financially supported by the National Natural Science Foundation of China (Grant No. 51108406), to whom we are grateful. We also thank Ms. Mao and Ms. Wu, the technician of 985-Institute of Agrobiology and Environmental Sciences of Zhejiang University, for help with N_2 adsorption–desorption, zeta potential and LC–MS measurements.

Appendix A. Supplementary data

Supplementary data associated with this article can be found, in the online version, at http://dx.doi.org/10.1016/j.apcatb.2012.08.014.

References

[1] V. Naddeo, S. Meric, D. Kassinos, V. Belgiorno, M. Guida, Water Research 43 (2009) 4019–4027.
[2] C.I. Kosma, D.A. Lambropoulou, T.A. Albanis, Journal of Hazardous Materials 179 (2010) 804–817.
[3] X. Yang, R.C. Flowers, H.S. Weinberg, P.C. Singer, Water Research 45 (2011) 5218–5228.
[4] P.J. Phillips, S.G. Smith, D.W. Kolpin, S.D. Zaugg, H.T. Buxton, E.T. Furlong, K. Esposito, B. Stinson, Environmental Science and Technology 44 (2010) 4910–4916.
[5] S.D. Kim, J. Cho, I.S. Kim, B.J. Vanderford, S.A. Snyder, Water Research 41 (2007) 1013–1021.
[6] M. Nassef, S.G. Kim, M. Seki, I.J. Kang, T. Nano, Y. Shimasaki, Y. Oshima, Chemosphere 79 (2010) 966–973.
[7] J.W. Kim, H. Ishibashi, R. Yamauchi, N. Ichikawa, Y. Takao, M. Hirano, M. Koga, K. Arizono, Journal of Toxicological Sciences 34 (2009) 227–232.
[8] S. Franz, R. Altenburger, H. Heilmeier, M. Schmitt-Jansen, Aquatic Toxicology 90 (2008) 102–108.
[9] P. Westerhoff, Y. Yoon, S. Snyder, E. Wert, Environmental Science and Technology 39 (2005) 6649–6663.
[10] M. Carballa, F. Omil, J.M. Lema, M. Llompart, C. Garcia-Jares, I. Rodriguez, M. Gomez, T. Ternesd, Water Research 38 (2004) 2918–2926.
[11] R. Shen, S.A. Andrews, Water Research 45 (2011) 944–952.
[12] J. Bai, Y.B. Liu, J.H. Li, B.X. Zhou, Q. Zheng, W.M. Cai, Applied Catalysis B: Environmental 98 (2010) 154–160.
[13] S.A. Snyder, S. Adham, A.M. Redding, F.S. Cannon, J. DeCarolis, J. Oppenheimer, E.C. Wert, Y. Yoon, Desalination 202 (2007) 156–181.
[14] P.M. Alvarez, J. Jaramillo, F. Lopez-Pinero, P.K. Plucinski, Applied Catalysis B: Environmental 100 (2010) 338–345.
[15] C. Martinez, M. Canle, M.I. Fernandez, J.A. Santaballa, J. Faria, Applied Catalysis B: Environmental 107 (2011) 110–118.
[16] R. Rosal, A. Rodriguez, M.S. Gonzalo, E. Garcia-Calvo, Applied Catalysis B: Environmental 84 (2008) 48–57.
[17] A.T. Stone, Environmental Science and Technology 21 (1987) 979–988.
[18] J.T. Ge, J.H. Qu, Journal of Hazardous Materials B100 (2003) 197–207.
[19] S. Bernard, P. Chazal, M. Mazet, Water Research 31 (1997) 1216–1222.
[20] Y. Dai, X.Y. Wang, Q.G. Dai, D. Li, Applied Catalysis B: Environmental 111 (2012) 141–149.
[21] M.H. Sui, J. Liu, L. Sheng, Applied Catalysis B: Environmental 111 (2011) 195–203.
[22] E.R. Stobbe, B.A. de Boer, J.W. Geus, Catalysis Today 47 (1999) 161–167.
[23] H.J. Ulrlch, A.T. Stone, Environmental Science and Technology 23 (1989) 421–428.
[24] D. He, X.H. Guan, J. Ma, X. Yang, C.W. Cui, Journal of Hazardous Materials 182 (2010) 681–688.
[25] B. Nowack, A.T. Stone, Journal of Physical Chemistry B 106 (2002) 6227–6233.
[26] H.C. Zhang, W.R. Chen, C.H. Huang, Environmental Science and Technology 42 (2008) 5548–5554.
[27] Z.J. Lu, K.D. Lin, J. Gan, Environmental Pollution 159 (2011) 2546–2551.
[28] G. Chen, L. Zhao, Y.H. Dong, Journal of Hazardous Materials 193 (2011) 128–138.
[29] M.J. Benotti, R.A. Trenholm, B.J. Vanderford, J.C. Holady, B.D. Stanford, S.A. Snyder, Environmental Science and Technology 43 (2009) 597–603.
[30] T. Gonzalez, J.R. Dominguez, P. Palo, J. Sanchez-Martin, Journal of Chemical Technology and Biotechnology 86 (2011) 121–127.
[31] X. Wang, Y.D. Li, Chemical Communications 7 (2002) 764–765.
[32] V. Subramanian, H.W. Zhu, R. Vajtai, P.M. Ajayan, B.Q. Wei, Journal of Physical Chemistry B 109 (2005) 20207–20214.
[33] K.S.W. Sing, D.H. Everett, R.A.W. Haul, L. Moscou, R.A. Pierotti, J. Rouquerol, T. Siemieniewska, Pure and Applied Chemistry 57 (1985) 603–619.
[34] Y.J. Chen, D.D. Dionysiou, Applied Catalysis B: Environmental 80 (2008) 147–155.
[35] Y.J. Chen, D.D. Dionysiou, Applied Catalysis A: General 317 (2007) 129–137.
[36] I.K. Konstantinou, T.A. Albanis, Applied Catalysis B: Environmental 49 (2004) 1–14.
[37] S.T. Yang, S.A. White, S.T. Hsu, Industrial and Engineering Chemistry Research 30 (1991) 1335–1342.
[38] E. Alkaya, S. Kaptan, L. Ozkan, S. Uludag-Demirer, G.N. Demirer, Chemosphere 77 (2009) 1137–1142.
[39] Y. Yoon, P. Westerhoff, S.A. Snyder, E.C. Wert, J. Yoon, Desalination 202 (2007) 16–23.

[40] H.C. Zhang, C.H. Huang, Environmental Science and Technology 37 (2003) 2421–2430.
[41] W.R. Chen, C.H. Huang, Environmental Pollution 159 (2011) 1092–1100.
[42] R.P. Liu, H.J. Liu, X. Zhao, J.H. Qu, R. Zhang, Journal of Hazardous Materials 176 (2010) 926–931.
[43] A. Manceau, B. Lanson, V.A. Drits, Geochimica et Cosmochimica Acta 66 (2002) 2639–2663.
[44] J.L. Junta, M.F. Hochella Jr., Geochimica et Cosmochimica Acta 58 (1994) 4985–4999.
[45] H.G. Yu, J.G. Yu, B. Cheng, Journal of Molecular Catalysis A: Chemical 253 (2006) 99–106.